AIAA 82-4136

Accuracy Potentials for Large Space Antenna Reflectors with Passive Structure

John M. Hedgepeth*
Astro Research Corporation, Carpinteria, Calif.

Analytical results indicate that a careful selection of materials and truss design, combined with accurate manufacturing techniques, can result in very accurate surfaces for large space antennas. The purpose of this paper is to examine these relationships for various types of structural configurations. Comparisons are made of the accuracy achievable by truss- and dome-type structures for a wide range of diameter and focal length of the antenna and wavelength of the radiated signal.

Introduction

LARGE antennas in space will eventually be needed. Not only will satellite-based communications require antennas of 100 m or more in diameter, but also will remote sensing demand even larger sizes. Some of the predicted needs are characterized in Fig. 1, taken from Ref. 1. Other studies predict larger apertures.

Large antennas will require some means of deployment, assembly, or fabrication in space, inasmuch as the Space Shuttle cannot accommodate their full bulk. In addition, the antennas must be built very accurately. The missions shown in Fig. 1 are seen to involve diameter-to-wavelength ratios of up to more than 100,000, with the majority centered around a ratio of 1000. For those missions for which the main beam must contain almost all the radiated energy, the emitted wave front must be accurate to 4% of the wavelength. These missions include all the Earth-directed antennas in which side-lobe gain must be kept very low. Even in the cases wherein the on-axis gain is of primary importance, the rms errors in the wave front are held to less than 12% of the wavelength. These missions include outward-pointed antennas for which the side-lobe gain can be relatively large.

In a reflector antenna, the wave-front error is very nearly twice the component of structural distortion normal to the reflector surface. Thus the surface error of a reflector antenna must be held to one-fiftieth of a wavelength for the low-side-lobe missions and one-sixteenth of a wavelength for the high-gain missions.

Combining the foregoing relationships with the data in Fig. 1 yields the requirement on structural surface accuracy. Submillimeter radio astronomy, for example, requires an accuracy of 1 ppm of the diameter. Those Earthward-pointed missions which have a diameter wavelength ratio of around 1000 require a surface accuracy of 20 ppm. At the other end, low-frequency radio astronomy allows the surface error to be as much as one-thousandth of the diameter.

The most straightforward way in which to achieve an accurate structure is to construct it of parts which are made precisely and which retain their dimensions throughout the life of the assembly. This "passive" approach avoids costly and time-consuming adjustment during assembly and yields long-term dimensional stability without the complication of active feedback control systems. It is the one of choice in those situations for which the resulting surface error is low enough.

Received Oct. 14, 1980; revision received Nov. 2, 1981.

*President. Fellow AIAA.

Clearly, the potential accuracy of antenna reflectors supported by passive structure is of interest when considering the feasibility and cost of future missions. The influence of fabrication tolerances on the surface accuracy is treated in Ref. 2. The purpose of the present paper (which is primarily a condensation of Ref. 3) is to investigate the influence of the accuracy requirements on the design geometry of the structure for four general types of structural configurations. Requirements on the panel sizes for a mesh reflector surface are obtained. The influence of fabrication imperfections on the surface error is evaluated. An initial look is taken of the effect of thermal strains on the accuracy. Finally, an evaluation is made of the diameter-wavelength ratios potentially feasible as limited by fabrication imperfections and thermal strains.

Structural Configurations

The type of spacecraft under consideration is shown in the center of Fig. 2. It consists of a reflector and a radio-frequency feed mounted at a distance by some sort of structure. Of course, the feed position and orientation with respect to the reflector is important, but in this paper attention is confined to the reflector portion only.

Four reflector configurations are shown in Fig. 2. These four are selected to encompass the types that utilize a knitted mesh material for the actual reflector surface. Such a material packages very well, is lightweight (~ 50 g/m^2), is compliant, and needs only to be positioned properly to be an excellent reflector.

The tetrahedral truss (see Fig. 3) has been discussed by many authors (see, for example, Ref. 4). Differences exist in

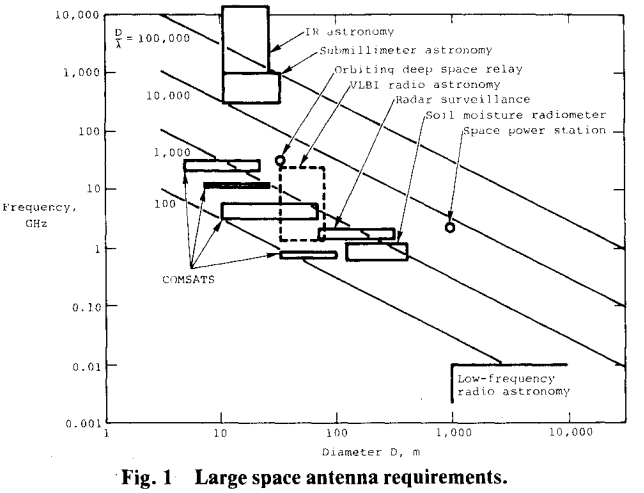

Fig. 1 Large space antenna requirements.

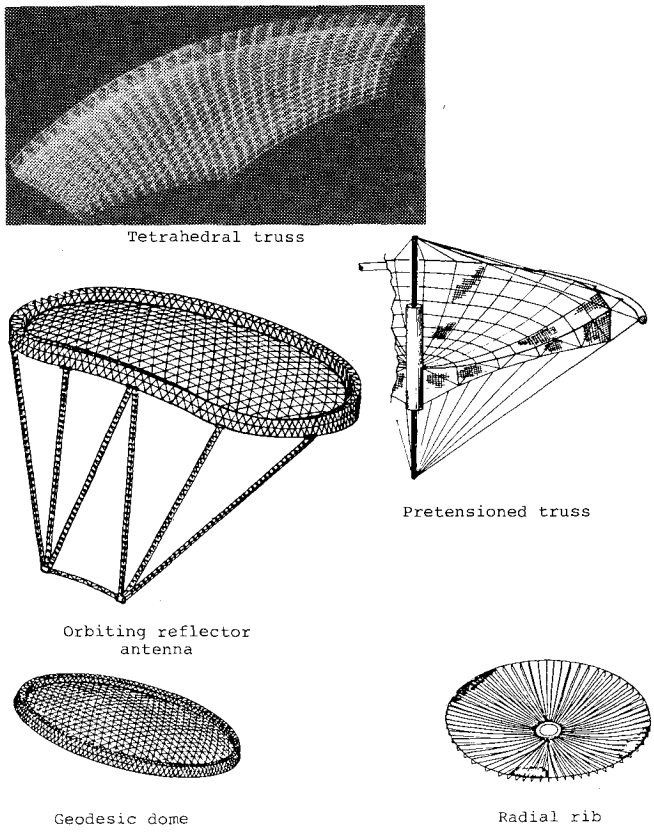

Fig. 2 Antenna structural configurations for mesh-type reflectors.

scale and in the manner in which the structure and the mesh interface. The structural members must be stiff enough to maintain sufficient straightness. Properly located joints allow stowage and deployment of the otherwise uncompliant structure. The mesh is assumed to be attached to the structure only along the truss surface elements.

The geodesic dome can be viewed as the limiting case of a tetrahedral truss as the depth H is reduced to zero. The geodesic dome behaves in the large as a membrane. It is simpler than the truss since only one surface of lattice elements is required. On the other hand, the membrane-like surface is very flexible unless the edge is supported by a stiff ring. Packaging and deploying the ring may present more difficulties than those presented by the more nearly uniform tetrahedral truss. The interface with the mesh is again assumed to be along the structural members.

The radial-rib configuration has as its structure a large number of radially oriented curved beams that are cantilevered from the central hub. The interface with the reflecting mesh is continuous along the chords of the beams. Thus the mesh is in gores rather than facets as is the case for the other configurations. The beams are stowed by wrapping them around the central hub with the necessary compliance supplied in a number of ways. The ATS-6 antenna is a salient example of this configuration.

The pretensioned truss shown in Fig. 4 is the author's version of the variously named "Maypole," "Hoop-and-Column," "Wire-Wheel," and "Spoked-Wheel' concepts. The basic structural element is the bicycle-wheel structure made up of the central column (hub) and the compression rim tied together by stays. The rim is articulated, allowing stowage. The central column is a deployable beam. The rest of the structure is "soft" in the sense that its elements need to carry tension only. Thus a variety of packaging techniques can be used without requiring complex joints. On the other hand, the deployed structure is "stiff." The tension-carrying elements are pretensioned sufficiently to allow incremental compression loading in orbit while retaining positive tension.

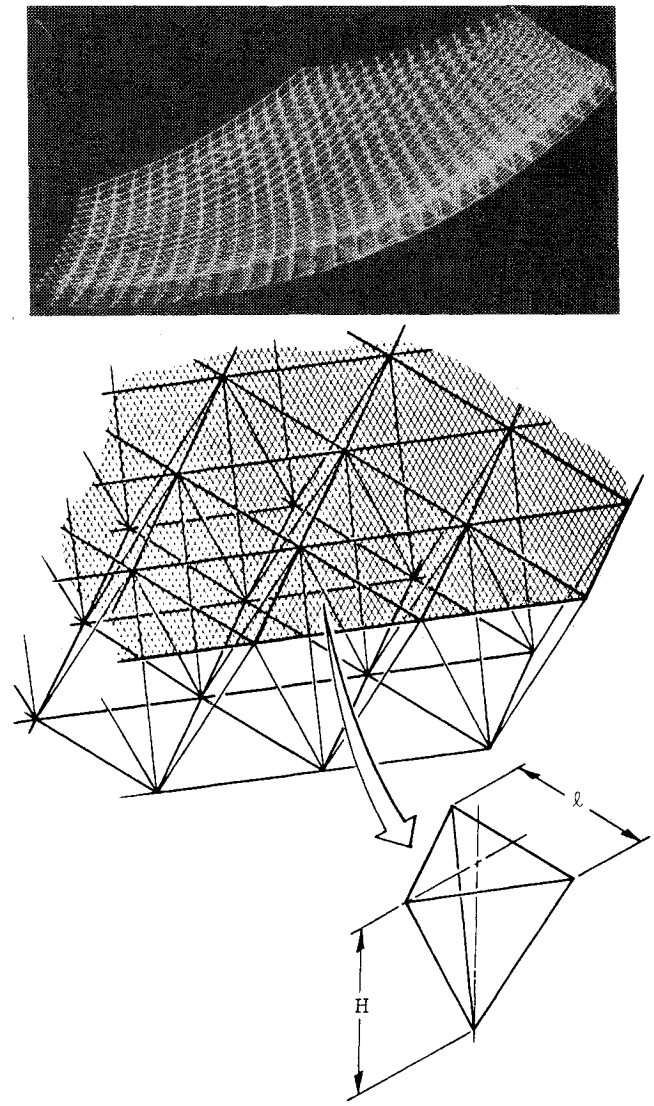

Fig. 3 Tetrahedral-truss configuration.

The members thus maintain their axial stiffness.

The reflector surface is formed by structural tension-stiffened radial beams. The tension in the curved chords automatically pretension the interchord members. The chord pretension is reacted by the compression rim. A compression spreader is needed at the outer end. The pretensioned beam is cantilevered at the central hub and also supported at the tip by the rim. Circumferential tension members provide the remainder of the structure. They and the upper chords of the beams are laced through the mesh to provide the necessary shaping to the reflector surface in quadrilateral facets. Note that the pretension in the members laced through the mesh must be sufficient to preclude objectionable bowing of these members.

Mesh Saddling

Since the mesh has very small bending stiffness, it behaves like a membrane; it can carry no compression. Furthermore, the tension must be reasonably uniform and isotropic in order to assure good electrical conductivity (and, hence, rf reflectivity) of the mesh. Values of around 2.5 N/m are used, for example, in the studies in Ref. 5.

A biaxially tensioned membrane with no lateral loading must have zero Gaussian curvature. Thus if the curvature in one direction is positive, the curvature in the other direction must be negative. Desired reflector surfaces are approximately spherical with a radius of curvature of twice the focal length F. Unfortunately, mesh surfaces want to look like

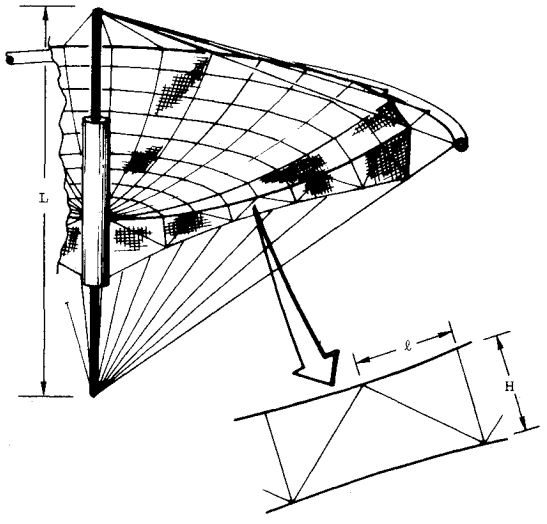

Fig. 4 Pretensioned-truss configuration.

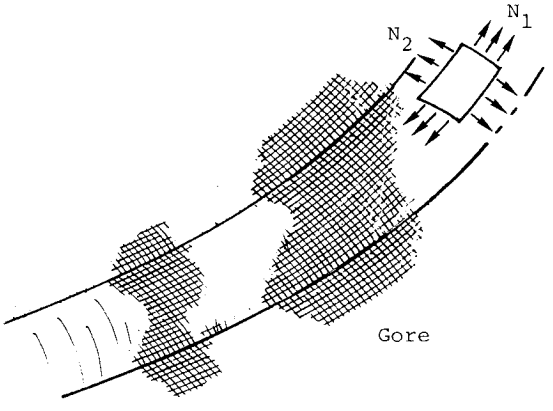

Fig. 5 Mesh saddling in the radial-rib concept.

saddles. Often, the mesh is pulled into a dish shape by a system of auxiliary chords attached to a number of interior points. This approach entails meticulous adjustment and therefore is specifically avoided in the present study.

The tension in the mesh also tends to curve the surface elements inward. The best approximation to a dish therefore is achieved by keeping the edges straight and, therefore, making the facets flat. The design geometry is adjusted to locate the corners (nodes) so as to cancel the average deviation between the flat and the desired curved surface. The rms deviation is kept small enough by limiting the size of the facets. Performing this process (see Ref. 3) yields, for a triangular facet

$$w_{\text{rms}} = 0.01614 l^2 / F \tag{1}$$

where w_{rms} is the root-mean-square value of the deviation between the sphere of radius $2F$ and the best-fit flat facet; F is the focal length; and l is the length of the facet side.

Solving for l yields

$$\frac{l}{D} = 7.87\sqrt{\frac{F}{D}\left(\frac{w_{\text{rms}}}{D}\right)_{\text{allow}}} \tag{2}$$

where D is the reflector diameter and $(w_{\text{rms}}/D)_{\text{allow}}$ is the design allowable surface-error ratio budgeted to this error source.

The facets in the pretensioned-truss design are approximately rectangular. For rectangular facets, the same

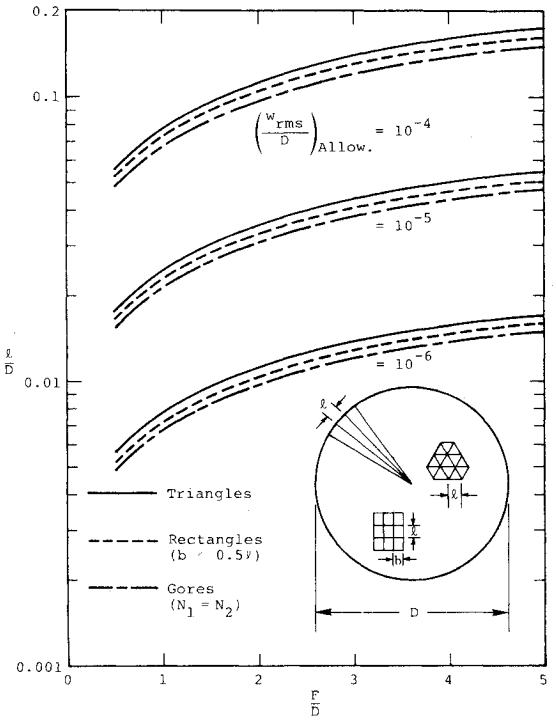

Fig. 6 Influence of focal-length ratio and allowable surface error on size of mesh panels.

process yields

$$\frac{l}{D} = 7.33\sqrt{\frac{F}{D}\left(\frac{w_{\text{rms}}}{D}\right)_{\text{allow}}}\left[1+\left(\frac{b}{l}\right)^4\right]^{-1/4} \tag{3}$$

where b is the smaller dimension of the rectangle and l is the larger.

For the radial-rib configuration, the mesh is in gores rather than facets. The curvature in the radial direction is enforced to be that of the rib. The saddling produces a negative curvature in the circumferential direction equal to N_1/N_2 times the radial curvature, where N_1 and N_2 are the membrane tensions in the radial and circumferential directions, respectively (see Fig. 5). The resulting rms deviation is

$$\frac{w_{\text{rms}}}{D} = 0.01076\,\frac{(l/D)^2}{F/D}\left(1+\frac{N_1}{N_2}\right) \tag{4}$$

where l is the gore width at the rim. For isotropic mesh tension, $N_1 = N_2$ and

$$\frac{l}{D} = 6.82\sqrt{\frac{F}{D}\left(\frac{w_{\text{rms}}}{D}\right)_{\text{allow}}} \tag{5}$$

for the gore configuration.

The facet and gore sizes are shown in Fig. 6. These curves can be used to determine the required degree of refinement of the structural geometry.

Effect of Fabrication Imperfections

Designing the geometry correctly is only the first step. The departure of the as-fabricated structure from the design must also fall within acceptable limits. Presumably, the effects of systematic fabrication imperfections can be removed by a combination of tooling and testing. There still remains the surface error due to random imperfections.

Beams

Consider constructing the beam shown at the top of Fig. 7 by assembling it from individual members, the length of each

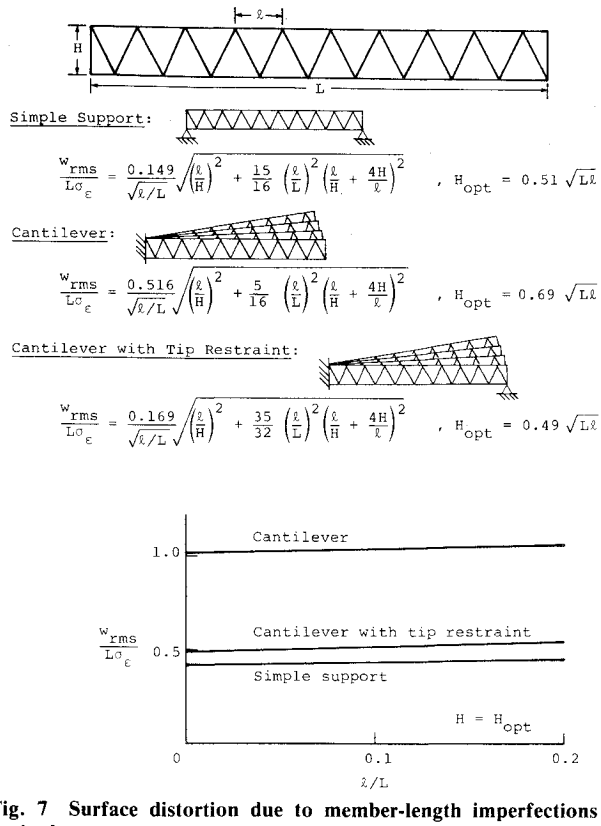

Fig. 7 Surface distortion due to member-length imperfections in lattice beams.

of which is a random variable with a mean of the design length and a standard deviation about that mean.

In Ref. 3, analyses are performed to determine the relationship between the rms surface error w_{rms} and the standard deviation σ_ϵ of the unit length errors for the elements of a beam. The results of these analyses are shown in Fig. 7. The following assumptions were made in obtaining the equations shown:

1) The value of the standard deviation of the length error is the same for all members.

2) The baylength l is small in comparison with the beam length L.

3) The surface error is measured from the "perfect" beam.

4) Inasmuch as the cantilever beams are envisioned as part of the radial-rib and pretensioned-truss configurations, the spatial average in these cases has been weighted by the radius in order to account properly for the larger areas of reflector near the rim.

In each expression, the first term under the radical represents the contribution of errors in the chord members, whereas the second term arises from the diagonal-member error. The first term is decreased by increasing the depth; the second term is increased for $H/l>0.5$. There exists an optimum depth which yields minimum error. This depth is shown by the equations and the resulting minimum error is shown in the graph in Fig. 7.

Note that supporting both ends of the beam yields a significantly smaller surface error than that obtained for the cantilever with a free tip. The large increase for the cantilever is due partly to the lack of tip constraint and partly to the heavier weighting of the average at the tip. If uniform weighting were used, the leading coefficient for the cantilever beam would be 0.408 rather than 0.516.

Trusses

The relationship between random fabrication imperfections and the surface error for a truss such as the tetrahedral truss is not nearly as straightforward to obtain as that for beams. The

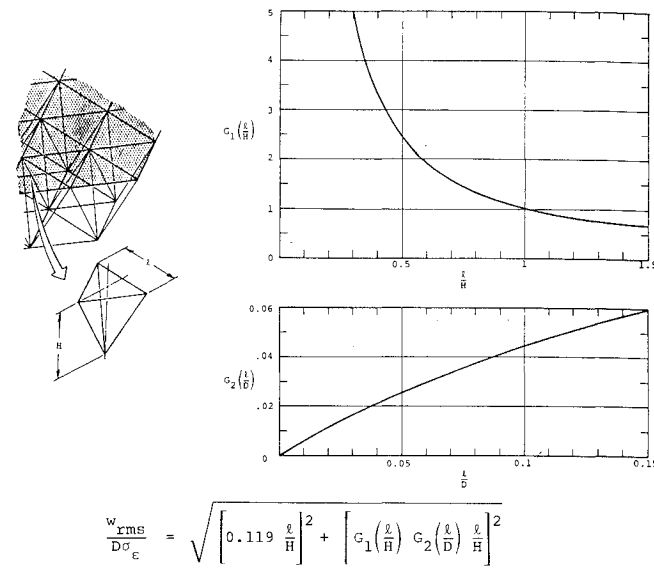

Fig. 8 Ratio of surface error to member-length error for tetrahedral truss.

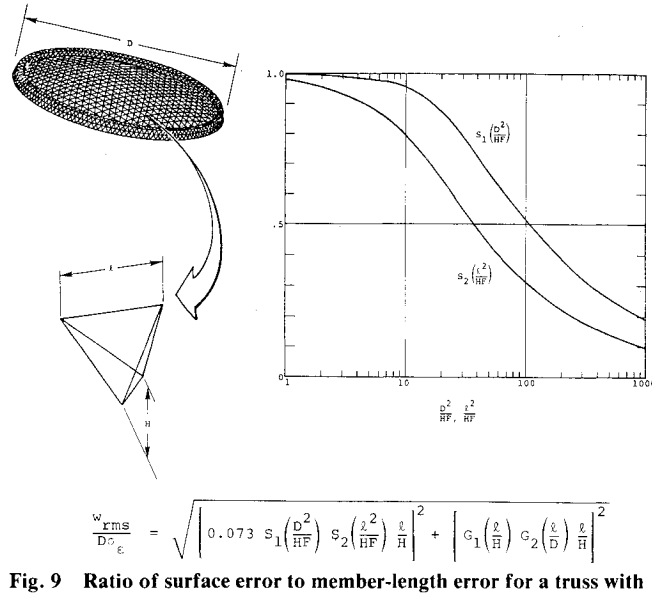

Fig. 9 Ratio of surface error to member-length error for a truss with error-free rim.

subject is treated in detail in Ref. 2, where the discovery of a useful analogy between the error analysis and natural-vibration analysis is reported. The results of that reference are shown in Figs. 8 and 9.

Figure 8 gives the rms error for a free-edged tetrahedral truss. It is assumed that moderate amounts of curvature cause little change in the vibration frequencies (and, hence, the surface errors) for the tetrahedral-truss configuration. Thus the results are directly applicable. Note that for $l \ll D$, the contribution of the second term under the radical (which arises from the intersurface members) is small. The resulting simplified expression is shown in Fig. 10 and used in Fig. 11.

Figure 9 applies to a curved truss shell with a rigidly held (zero error) rim. For such a configuration, the influence of curvature can be very important, particularly for thin trusses (see Ref. 2).

The error estimation for the geodesic dome was obtained in Ref. 2 as a limit of the curved-shell results as the shell depth approached zero. The appropriate error expression is shown in Fig. 10 and is plotted in Fig. 11. Note that the results shown on these two figures are greater by a factor of 2 than those erroneously reported in Ref. 3.

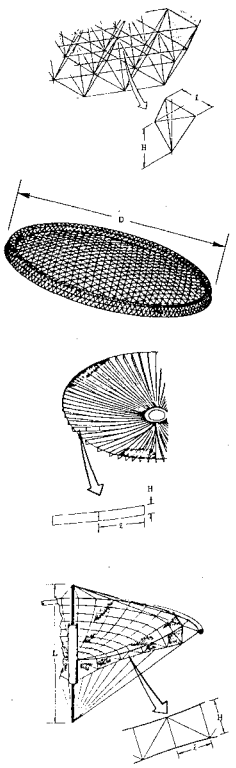

Tetrahedral truss:

$$\frac{w_{rms}}{D} = 0.12 \frac{\ell}{H} \sigma_\varepsilon$$

Geodesic dome:

$$\frac{w_{rms}}{D} = \frac{2F}{D} \sigma_\varepsilon$$

Radial rib:

$$\frac{w_{rms}}{D} = 0.183 \sqrt{\frac{D}{\ell}} \frac{\ell}{H} \sigma_\varepsilon$$

Pretensioned truss:

$$\frac{w_{rms}}{D} = \sqrt{\left[0.060 \frac{\ell}{H}\right]^2 \frac{D}{\ell} + \left[\frac{w_{dia}}{D}\right]^2 + \left[\frac{w_{rim}}{D}\right]^2} \sigma_\varepsilon$$

$$\frac{w_{dia}}{D} = \frac{1}{2} \sqrt{\frac{\ell}{D}} \left(\frac{H}{\ell} + \frac{1}{4} \frac{\ell}{H}\right)$$

$$\frac{w_{rim}}{D} = 0.177 \left(\frac{D}{L} + \frac{L}{D}\right)$$

Fig. 10 Equations for estimating surface error due to random member-length imperfections for the four configurations.

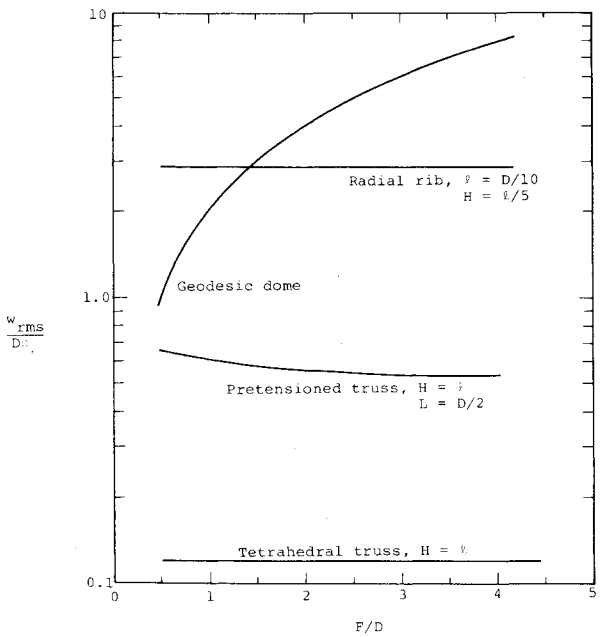

Fig. 11 Error ratios for the four configurations, $(w_{rms}/D)_{allow} = 10^{-5}$.

Application to Example Configurations

The appropriate error equations for the tetrahedral-truss and geodesic-dome configurations are derived as previously described and shown in Fig. 10. Note that the averages employ uniform weighting over the surface area. While it is recognized that more accurate results could be obtained if the weighting were made proportional to the illumination, the present uniform-weighting results should be useful.

For the radial-rib configuration, an appropriate approach is to use the cantilever-beam expression from Fig. 7, with $L=D/2$ and l defined as being the correlation length of fabrication errors. The depth will ordinarily be much less than l. Thus the "diagonal" contribution can be neglected. The resulting expression is shown in Fig. 10. If the radial rib is of a truss configuration, then the correlation length is equal to the baylength. If, on the other hand, the rib is in the form of a segmented lenticular tube, the correlation length is the segment length.

For the pretensioned-truss configuration, the surface error is assumed to be approximated by the error in the radial pretensioned truss beams. Note that the expression in Fig. 10 includes a contribution due to the inaccuracy of the rim itself induced by stay-length errors. For reasonably deep radial trusses, the rim error predominates.

The error results are compared for the four configurations in Fig. 11. The lowest-error configuration is the tetrahedral truss, shown for a value of H/l equal to unity.

The next most favorable configuration is the pretensioned truss for higher F/D ratios. Here again, the depth H is set equal to l, where l is obtained from Fig. 6 for $(w_{rms}/D)_{allow} = 10^{-5}$. The central hub length is chosen arbitrarily to be one-half the diameter.

The geodesic dome exhibits reasonable error performance only for the smaller F/D ratios. For $F/D = 0.5$, it is of interest because it involves many fewer members than does the tetrahedral truss.

The radial-rib design is very attractive in its simplicity. Furthermore, the configuration is flight proven in several versions. Unfortunately, the configuration is quite error sensitive, as seen by the curve in Fig. 11 where l is taken to be $D/10$ and the rib depth H is assumed to be one-fifth the correlation length. This configuration can be made attractive by designing the rib depth to be large, an approach not suggested in the past. Otherwise, its usefulness for the more demanding missions is questionable.

Fabrication Tolerances

Throughout this section, the surface errors are related to the standard deviation of the unit member-length error. This latter quantity is at the control of the designer, although with a considerable cost impact. In general, a value of σ_ε of 10^{-3} is representative of ordinary careful practice, 10^{-4} is characteristic of a high-quality machine shop, 10^{-5} is achievable with well-designed and operated hard tooling, and 10^{-6} is very difficult and costly.

Fortunately, the attractive configurations allow a much better surface-accuracy ratio than the unit member-length accuracy.

Environmental Strains

The antenna must remain accurate in the presence of environmental effects after it is established in space. It is assumed that materials will be available with the necessary dimensional stability in the vacuum, *UV*, and particulate radiation environment that exists in orbit. Furthermore, it is assumed that redundant design will be used to resist the deleterious effects of meteoroids. Similarly, the influence of load-induced strains and the uncertainty in such strains can be kept to acceptable limits by proper design. (Indeed, this latter requirement is probably the overriding design criterion.) But there remains the ubiquitous effects of thermal strains.

The influence of thermal strains on surface accuracy is complex and dependent to a great extent on detailed design. There are some overall preliminary considerations worthy of mention herein. Attention is restricted to the tetrahedral-truss structure inasmuch as it exhibits the most potential for accurate reflectors.

Thermal Transient

Concern has been expressed about the loss in antenna accuracy when entering or leaving the Earth's shadow. This can be characterized first as a major change in average temperature. The static consequences of this change are treated in the following section. The dynamic effects can be

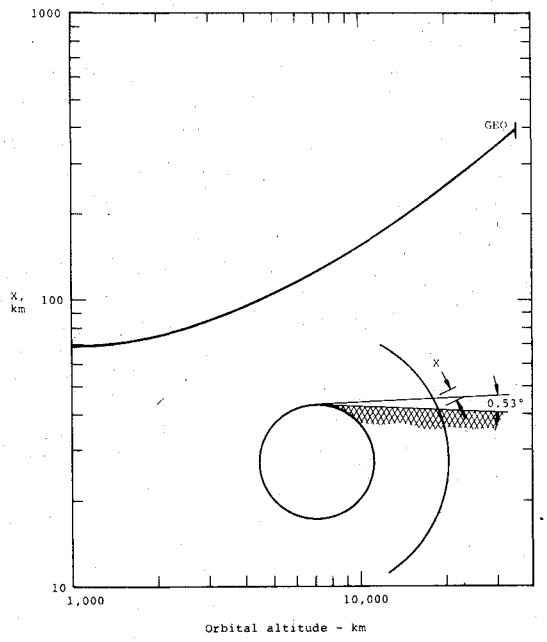

Fig. 12 Length of sun-shadow transition.

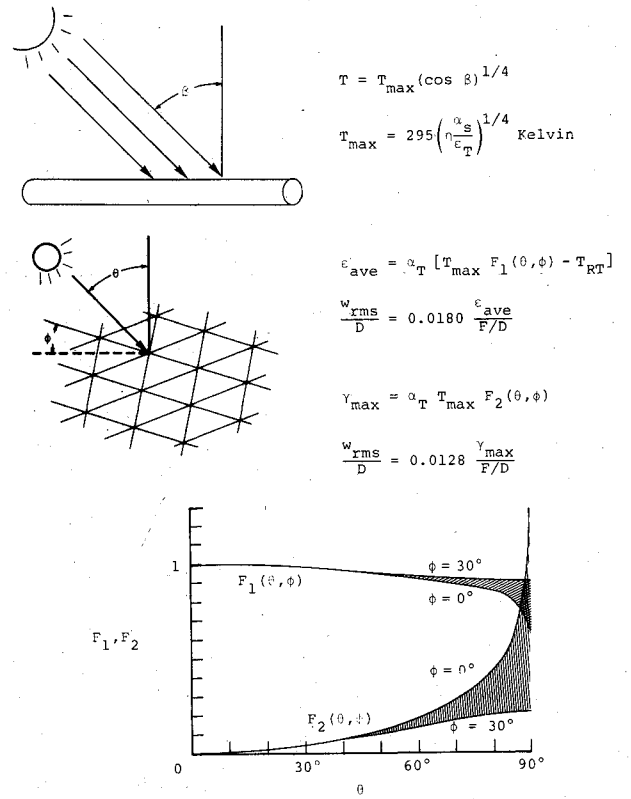

Fig. 13 Geometrical effects on thermal strains.

no more than twice as much in total. Second, the various portions may change temperature at different rates. Care must of course be exercised to ensure that the thermal inertias of various important structural members do not differ widely enough to cause problems. Note that temperature variations in the structure due to the spatial gradient in the thermal environment itself will be very small, as can be seen in Fig. 12. Here the length of the orbital path in the penumbra is shown as a function of orbital altitude. Even for low orbits, the length of the penumbra is more than 60 km. The gradient of solar intensity is, therefore, small for the structural dimensions under consideration herein.

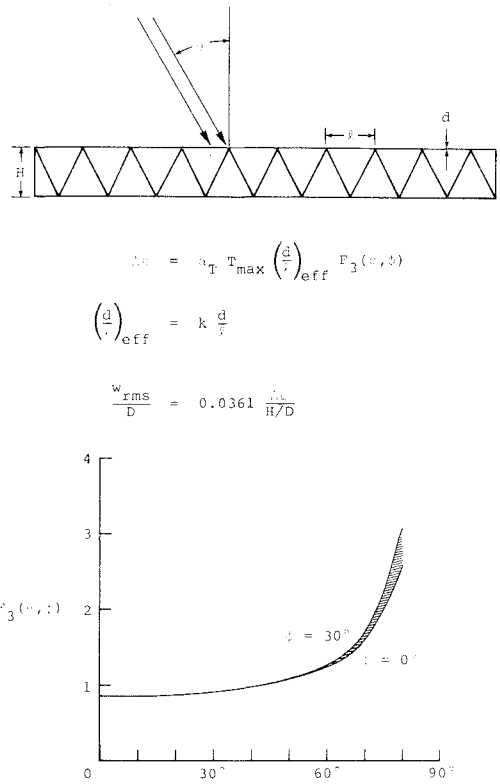

Fig. 14 Effect of self-shading for tetrahedral truss.

Thermal Strains

Of more significance are the variations in temperatures and, hence, thermal strains in the various structural members. In the upper part of Fig. 13 is shown the radiation equilibrium temperature for a circular rod illuminated by the sun. The factor η represents the reduction in the solar constant due to shadowing, and α_s/ϵ_T is the familiar absorptivity-emissivity ratio.

When the sun shines on a triangular grid of elements, some of them are hotter than the others because their axes are more nearly normal to the solar radiation. The differing temperatures cause differing strains in the members of differing orientation. The strains can be expressed in terms of equivalent biaxial membrane strains and completely defined by the average strain ϵ_{ave} and the maximum shear strain γ_{max}. Expressions for these quantities are shown in Fig. 13, where α_T is the thermal-expansion coefficient.

The effect on surface error of the average strain can be obtained by recognizing that the strain changes the radius of curvature of the reflecting surface from $2F$ to $2F(1+\epsilon_{ave})$. The resulting rms deviation from the original surface (with zero mean, of course) is given by the expression in Fig. 13. Note that T_{max} is approximately equal to the room temperature at which the structure is originally sized. The average-strain effects are, therefore, most important when the reflector gets very cold.

The effect on surface error of the maximum shear strain is to warp the surface into a shape similar to that obtained when diametrically opposite rim points are squeezed together.

The corresponding rms surface error is as expressed in Fig. 13. Note that the maximum effect is experienced when the sun is edge-on ($\theta = 90$ deg) and parallel to one of the sets of members.

Another source of thermal gradient is the temperature difference between the two faces of the tetrahedral truss due to shading on one face by the other—and by the intersurface members. This problem has been analyzed with results as shown in Fig. 14. The amount of shading depends, of course, on the slenderness of the truss members. (Note that shading

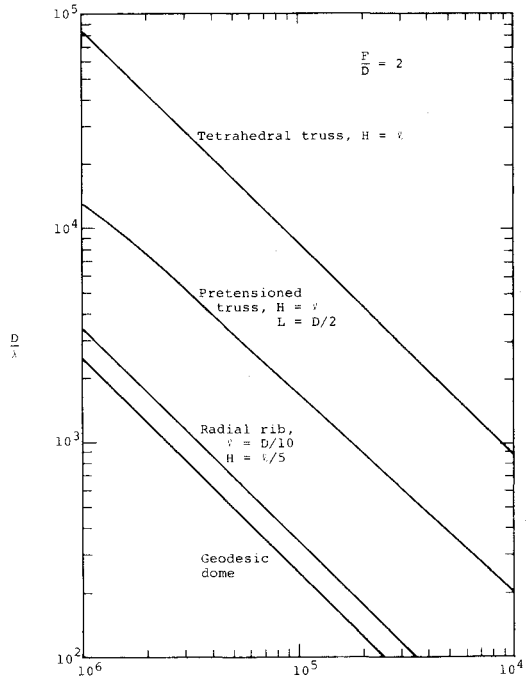

Fig. 15 Potential antenna sizes for $w_{rms} = \lambda/100$ as limited by fabrication imperfections.

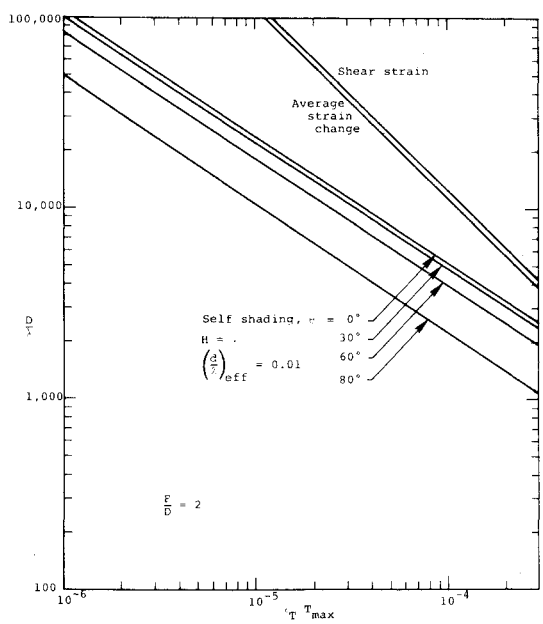

Fig. 16 Potential tetrahedral-truss antenna sizes for $w_{rms} = \lambda/100$ as limited by thermal strains.

due to the mesh is assumed to apply uniformly to both surfaces.) The analysis is linearized with respect to d/l and is, therefore, only accurate for low d/l. It considers only shading due to the surface members. The shading due to the intersurface members is included approximately by the factor k in the expression for the strain differential.

The maximum shading effect is obtained when the sun strikes the surface perpendicular to a set of members. Total blocking is achieved for glancing illumination. Of course, this situation is unrealistic for the curved dishes under consideration. For this reason, the curves are cut off at $\theta = 80$ deg. Note that F_3 includes both the effect of shading and the average-strain effect described in Fig. 13.

Other Thermal Effects

It is recognized that the foregoing constitutes only a beginning in the understanding of the influence of thermal effects. For example, the influence of thermal-strain differentials of the intersurface members should be investigated. The effects that are considered should, however, be useful in evaluating the magnitude of the thermal effects.

Concluding Discussion

In order to illustrate the overall consequences, the results in Figs. 15 and 16 are presented. Here the achievable antenna ratio of diameter to wavelength is plotted vs the fabrication tolerance parameter σ_ϵ and the maximum thermal strain parameter $\alpha_T T_{max}$. The criterion in both cases is that the surface distortion shall be limited by one-half of the allowable $\lambda/50$ that is the requirement for most of the missions described in Fig. 1. This is done in order to allow the various sources of error (which are, in general, additive on a mean-square basis) to coexist and still be able to meet the $\lambda/50$ requirement.

A particular focal-length-to-diameter ratio of 2 is chosen for the comparison. Most antennas with electronically steerable beams will require such a high F/D.

As can be seen in Fig. 15, the tetrahedral truss is by far the most attractive configuration for attainment of large apertures with acceptable error due to fabrication imperfections. A value of D/λ of nearly 10,000 is possible for a fabrication tolerance parameter of 10^{-5}. Reference to Fig. 1 shows that this ratio would encompass all the missions except those involving submillimeter and i.r. astronomy. And if the relaxed $\lambda/16$ criteria were used, a value of $D/\lambda = 30{,}000$ would be feasible. Thus even submillimeter astronomy is possible from this standpoint.

The pretensioned truss is probably more readily packaged than the tetrahedral truss. It shows good accuracy for most of the missions.

Even the geodesic dome and a radial-rib design present usable accuracy for the smaller-aperture communication-satellite missions. Note that the potential of the radial-rib design would be improved by using a deeper rib.

As can be seen from Fig. 16, the temperature differences between surfaces could be a severe limiter on the antenna sizes for the tetrahedral truss, the effects being much more severe than either overall temperature-strain effects or shear-strain effects. For a nominal worst case of $T_{max} = 295$ K and α_T of 0.5×10^{-6}/K (readily achieved for graphite/epoxy), the limiting value of D/λ is 1000. In order to achieve the D/λ of 10,000, of which the tetrahedral truss is otherwise capable, an order of magnitude improvement would be required. This could be accomplished through a combination of deepening the truss, making the members more slender (perhaps not feasible if loading is already high), reducing the absorptivity-emissivity ratio, and finally, developing a more stable material. Much remains to be done in this area.

Acknowledgment

This work was performed under Contract NAS1-15347 from NASA Langley Research Center.

References

[1] Powell, R.V., "Introduction to Large Space Antenna Session of Workshop on Space Radio Astronomy," JPL Internal Paper, Charlottesville, Va., June 27, 1979.

[2] Hedgepeth, J.M., "Influence of Fabrication Tolerances on the Surface Accuracy of Large Antenna Structures," *AIAA J.*, Vol. 20, May 1982, pp. 680-686.

[3] Hedgepeth, J.M., "Accuracy Potentials for Large Space Antenna Structures," SAWE Paper 1375, May 1980.

[4] Fager, J.A., "Large Space Erectable Antenna Stiffness Requirements," *Journal of Spacecraft and Rockets*, Vol. 17, March-April 1980, pp. 86-92.

[5] Montgomery, D.C. and Sikes, L.D., "Development of the Maypole (Hoop/Column) Deployable Reflector Concept for Large Space Systems Applications," NASA CP-2118, Nov. 1979.